Research on Tribological Properties of H13 Steel of Shield Machine Hob by Laser Shot Peening

Yifeng Zhang
University of Jinan
XueFeng Yang (wshytzh@163.com)
University of Jinan
Shouren Wang
University of Jinan
Wanyang Li
University of Jinan
Qiang Wu
Shandong Tongchuang Auto Cooling System Co., Ltd
Wangliang Zhao
Shandong Tongchuang Auto Cooling System Co., Ltd
Yang Gao
Shandong Tongchuang Auto Cooling System Co., Ltd
Kai Wang
Qingdao Sufa New Material Co., Ltd

Research Article

Keywords: laser shot peening, simulation, tribological properties

Posted Date: November 8th, 2021

DOI: https://doi.org/10.21203/rs.3.rs-1026775/v1

Version of Record: A version of this preprint was published at The International Journal of Advanced Manufacturing Technology on January 23rd, 2022. See the published version at https://doi.org/10.1007/s00170-021-08578-y.

Abstract

In this paper, the laser shot peening technology of H13 steel is studied to improve the friction and wear performance of shield machine hob. And to utilize the laser shot peening (LSP) experiment and simulation analysis, the influence of LSP parameters on the friction and wear performance of H13 steel after strengthening is studied. The results show that the residual stress and the depth of stress layer are increased after LSP, which is beneficial to reduce the friction and wear of material surface. In addition, the surface has a paint absorption layer which can absorb laser energy to avoid surface annealing. The maximum residual stress of H13 steel is 911 MPa and the hardness is 650.7 HV, when there are three-times of black paint absorption and LSP. Compared with the raw material, the residual stress is increased by 125% and the hardness is increased by 18%. And its friction coefficients and wear volume were relatively lower than other schemes. The average friction coefficient and wear volume were reduced by 10.8% and 57.2% respectively.

1 Introduction

The cutter ring of the shield machine is the key part of the shield machine, and it is also the most easily worn part in the working process. At present, H13 steel is mainly used to manufacture the cutter ring of shield machine. Telasang[1] deems H13 steel has high toughness, hardenability, cold and hot fatigue resistance, and is not easy to produce hot fatigue cracks. However, Ren[2] analysis the cutter made of H13 steel has some defects such as eccentric wear, fracture and wear. At present, the main strengthening methods of H13 steel are laser surface strengthening, Jia[3] through laser surface melting strengthened the H13 steel. And Dadoo[4] has used TiC composite coating to strengthened the surface hardness belong the surface additive strengthening. Yang[5] and Liu[6] respectively have used the boronizing and nitriding to strengthen the H13, so these are also commonly used for surface strengthening of H13 steel. Hu[7] deems the LSP is a kind of surface modification technology using short pulse laser beam. The LSP on 7075-aluminum alloy surface was studied by Wang[8] the authors concluded that LSP is an effective approach to decrease the depth and width of wear scars, and to reduce the abrasion loss in seawater environment. These observations were attributed to the grain refinement during LSP which increases the surfaces hardness and abrasion resistance. Ren[9] has researched laser shock peening to reveal the effects on Cr12 microstructures and fatigue resistance. These results show a deep layer of compressive residual stress is developed by laser shock peening by Angulo[10], and ultimately the isothermal stress-controlled fatigue behavior is enhanced significantly. Kyun[11] through the shot peening H13 steel to improve the hardness and the residual compressive stress. The residual compressive stress increases, and the toughness of the material increases.

Through the above research by all researchers, LSP technology has not been applied to H13 steel of shield machine hob. Research on tribological properties of H13 steel of shield machine hob by Laser shot peening, has great significance to the study of LSP strengthen high load tools.

2 Simulation Model

2.1 Material model

The material H13 steel used in the experiment is medium carbon steel. After quenching 1313K and secondary tempering 853K, the material performance is the best. And the performance parameters are shown in Table 1.

Table 1 Performance parameters of H13 steel

ρ (Kg/m^3)	v	E (MPa)	σ_Y^S (MPa)	σ_Y^D (MPa)
7870	0.29	211000	1695	2500

LSP simulation is dynamic analysis, so the J-C constitutive model of H13 steel is used. The J-C constitutive model parameters are shown in Table 2.

Table 2 The J-C constitutive model of H13 steel

Initial yield stress (MPa)	Hardening constant (MPa)	Strain rate constant	Hardening exponent	Thermal softening exponent
1695	1088	0.0048	0.6272	0.52

The size of specimen is 40 mm × 40 mm × 15 mm. The hardness is about 550 HV, and the residual compressive stress is 420 MPa.

2.2 Pressure model of laser shot peening

Lu[12] has explained the theory of LSP. High energy laser beams pass through the confinement layer of the material surface and irradiate the absorption layer of the material. After absorbing a lot of laser energy, high pressure plasma will be produced. Due to the existence of the confinement layer, the plasma forms stress waves. Under the action of stress wave, plastic deformation occurs. Meantime, the near surface microstructure of the material has refined by the stress wave and the compressive stress is produced. The hardness of material would increase, as the result of microstructure was refined. The theory of LSP as shown in Fig. 1.

When the laser induced wave propagates in the target, the peak pressure (*P*) of the LSP exceeds the Hugoniot Elastic Limit (*HEL*) of the target, the plastic deformation of the target surface occurs by Prabhakaran[13]. *HEL* estimation mathematical model formula:

$$HEL = \sigma_Y^D \frac{1-v}{1-2v} \qquad (1)$$

Substituting the parameters into the solution: *HEL* (H13) = 4093 MPa. When P_{max} = 2~2.5 *HEL*, the material has permanent deformation in study of Shukla[14]. The laser pulse width is 20 ns, and the

pressure model of LSP as shown in Fig. 2. The simulation model of LSP as shown in Fig. 3.

3 Experimental Design

3.1 Theory of laser shot peening

LSP is a transient process, so it is impossible to accurately experiment and calculate the pressure produced by laser beam impacting the target. In order to estimate the pressure produced by shock wave, Fabbro[15] has proposed a formula for estimating the peak pressure of shock wave on the target surface.

$$P = 0.01\sqrt{\frac{\alpha}{2\alpha+3}}\sqrt{Z}\sqrt{I_0} \tag{2}$$

Where α is the ratio of thermal to internal energy, when the black paint as absorptio layer, which is 0.3. The acoustic impedance of water is 2.39×10^5 g/cm^2·s. The acousic impedance of H13 steel is 45.8×10^5 g/cm^2·s.

Z represents the total impedance of the constraint layer and the target material, which is determined by the constraint layer impedance ($Z_{overlay}$) and the target impedance (Z_{target}) together.

$$\frac{2}{Z} = \frac{1}{Z_{overlay}} + \frac{1}{Z_{target}} \tag{3}$$

I_0 represents laser power density.

$$I_0 = \sqrt{\frac{E}{\frac{\pi d^2}{2}\tau}} \tag{4}$$

There E is the laser pulse energy. The d is Laser spot diameter and the τ is laser pulse width.

3.2 Experimental scheme

Ys80-r200b LSP equipment was used for LSP treatment, and the LSP parameters as shown in the Table 3. The processing path of LSP as shown in Fig. 4.

Table 3 LSP treatment parameters

Laser energy	Laser spot diameter	Laser pulse width	LSP scheme		
			1	2	3
7 J	2.4 mm	20 ns	Black paint absorption LSP once	Black paint absorption LSP three-times	No absorption LSP three-times

After LSP, the sliding friction and wear behaviors between H13 steel and GCr15 Bearing Steel (the diameter of 6.35 mm, the hardness of 750 HV) under different pressures were studied by RTEC multifunctional friction and wear tester (MFT-50, San-Jose, CA, USA). The schematic diagram of friction and wear tester as shown in Fig.5. The experimental parameters are as follows: load 75 N and 100 N (the pressure ranges from 300 MPa to 400 MPa), amplitude 4.5 mm, frequency 4 Hz, time 60 min. The friction coefficient and the experimental temperature were monitored in real time by the matching program of the testing machine. The wear profile and wear volume were measured by USP sigma white light interferometer (USP-Sigma, Saint Louis, MO, USA). The morphology of wear mark, residual stress, and hardness were observed by X-ray stress meter (iXRDCOMBO, Proro, Canada) and micro Vickers hardness meter (402-MVD, Wilson, Norwood, USA).

4 Result And Discussion

4.1 Simulation result

The simulation analysis uses ABAQUS software. Firstly, the dynamic response of H13 steel model under LSP was analyzed in the display integration module, and then the static rebound was carried out in the implicit integration module. In case of multiple LSP, the interval static rebound time is the interval time of machining. The final rebound time is 1000 times of the dynamic response time, which makes the material fully rebound.

In Fig. 6-(a), the trend of residual stress of H13 steel is studied by changing the pressure and times of LSP wave. When the pressure increases from 4 GPa to 12 GPa by LSP once, the maximum residual pressure stress and the maximum residual tensile stress show an increasing trend. The pressure stress increases from -472 MPa to -1204 MPa, and the tensile stress increases from 111.7 MPa to 690.4 MPa. In Fig. 6-(b) shows the residual strain corresponding to LSP once. With the increase of shock pressure, the strain increases from 0.013 to 0.139. When the three-times LSP pressure increases from 4 GPa to 12 GPa, the maximum residual pressure stress and the maximum residual tensile stress show an increasing trend. The pressure stress increases from -744.7 MPa to -1652 MPa, and the tensile stress increases from 190.8 MPa to 1019 MPa. Fig. 6-(b) also shows the residual strain corresponding to three-times of LSP. With the increase of LSP pressure, the strain increases from 0.033 to 0.436. It can be concluded that the residual stress and strain increase with the increase of LSP pressure.

However, H13 steel shows 420 MPa residual pressure stress, when the LSP residual tensile stress is greater than 420 MPa, the specimen will have residual tensile stress, and the occurrence of participating tensile stress will lead to cracks in the material. Therefore, in the LSP simulation, the LSP pressure cannot be greater than 8 GPa (residual tensile stress is 441.6 MPa) in once and 7 GPa (residual tensile stress is 461.8 MPa) in three-times.

In Fig. 7, it has shown the residual stress and strain of different LSP pressure. It can be seen that with the increase of LSP pressure, the influence layer of residual stress increases by about 0.2 mm. With the same

residual stress, the deeper the stress layer, the stronger the LSP toughness. In Fig. 7-(a), the residual stresses of LSP three-times by 6 GPa have approximately equaled to the LSP once by 8 GPa. And the pressure layer of LSP once by 8 GPa is about 0.4 mm deeper than LSP three-times by 6 GPa. Its strain is about 0.02, and its smaller than LSP three-times by 6 GPa from the Fig. 7-(b). When it maintains the same LSP pressure, with the LSP times increase, the residual stress and stress layer increase. Therefore, it can be concluded that the LSP pressure is larger and the pressure layer is deeper at one time. The residual stress is larger and the stress layer is deeper at three-times.

4.2 Experimental Result

The residual stress increases with the increase of LSP pressure. Excessive residual stress is easy to cause cracks and reduce the service performance. In order to obtain large residual stress without crack, the required laser energy and spot size are calculated with 6 Gpa as LSP pressure. After LSP processing, the surface morphology of the material as shown in the Fig. 8-(a), (b), (c), and (d) respectively correspond to the raw material, once LSP by black paint absorption, three-times LSP by black paint absorption, and three-times LSP of no absorption. It can be seen that the deformation of specimen (c) is larger than the others.

4.2.1 Micro-hardness

The hardness of the material was tested by micro-hardness tester. The hardness of the surface was randomly taken from 15 points, and the average hardness was obtained by removing the maximum value and the minimum value. In Fig. 9-(a), the a, b, c, and d respectively correspond to the raw material, once LSP by black paint absorption, three-times LSP by black paint absorption, and three-times LSP of no absorption, which hardness are about 550 HV, 616 HV, 650.7 HV, and 629.36 HV respectively. Compared with the hardness, it can be concluded that the strengthening effect is the best when the black paint absorption and LSP for three-times, the hardness is increased by 100.7 HV and the strengthening effect is about 20.13%. In terms of hardness, the scheme of three-times LSP of black paint absorption is the best.

4.2.2 Residual stress

The residual stress of the material was measured by X-ray stress measuring instrument. The residual stress of 15 points was randomly selected on the surface. In Fig. 9-(b), the a, b, c, and d respectively correspond to the raw material, once LSP by black paint absorption, three-times LSP by black paint absorption, and three-times LSP of no absorption. According to the Fig. 9-(b), the residual compressive stress of the a is 420 MPa. The residual compressive stress of the c is the largest, about 911 MPa. The residual stresses of the b and c are approximately equal. The residual stress and simulation stress of the c combined with the residual stress of the a, can be obtained that the experiment and simulation results are approximately equal. The b is the once LSP, its residual stress layer of the specimen is small, and the maximum residual stress appears near the surface layer. The residual stress measured by X-ray residual stress measuring instrument is the maximum residual stress of the material, which is equivalent to the simulation. However, the residual stress of the d has quite different from the simulation results. The

reduction of the residual compressive stress in the d is due to the annealing effect of high energy laser irradiation on the sample without absorption layer. From the aspect of residual stress, the scheme of three-times LSP with black paint absorption (the c) is the best.

4.2.3 Friction coefficient

(1) Average friction coefficient

After LSP to strengthen H13 steel, the friction experiments were carried out by the friction and wear testing machine. Each experiment parameter is repeated three-times to obtain the stable friction coefficient and calculate the average friction coefficient. Fig. 10-(a) shows the average friction coefficient of the raw material, once LSP by black paint absorption, three-times LSP by black paint absorption, and three-times LSP of no absorption. And the initial pressure is 75 N and 100 N in fiction. When the initial pressure is 75 N, the friction coefficient of black paint absorption LSP three-times is 0.4091 that is the lowest, and the raw material is 0.4601. The results are consistent with the trend of hardness. The reason for this phenomenon is that the highly hardness of material and relative fine grains. And when the initial pressure is 100 N, the friction coefficients become increase, but the trend is consistent with the hardness. The reason for the increase in friction coefficient is that when the initial pressure increases, the friction type and w

After LSP to strengthen H13 steel, the friction experiments were carried out by the friction and wear testing machine. Each experiment parameter is repeated three-times to obtain the stable friction coefficient and calculate the average friction coefficient. Fig. 10-(a) shows the average friction coefficient of the raw material, once LSP by black paint absorption, three-times LSP by black paint absorption, and three-times LSP of no absorption. And the initial pressure is 75 N and 100 N in fiction. When the initial pressure is 75 N, the friction coefficient of black paint absorption LSP three-times is 0.4091 that is the lowest, and the raw material is 0.4601. The results are consistent with the trend of hardness. The reason for this phenomenon is that the highly hardness of material and relative fine grains. And when the initial pressure is 100 N, the friction coefficients become increase, but the trend is consistent with the hardness. The reason for the increase in friction coefficient is that when the initial pressure increases, the friction type and wear morphology of the experiment piece change.

ange.

(2) Friction coefficient

Figure 10-(b) shows friction coefficient of the friction process. In the friction process, except for early fluctuations, the overall trend is the same as that of hardness. As the friction zone enters the bottom layer of the point region, the hardness of the material in this region is uniform, and the friction coefficient tends to be stable. After initial fluctuation, the friction coefficient is stable at 0.4215. Because the black paint absorption LSP once, the surface hardness of the sample is low, and the friction coefficient is large. At the same time, the wear gradually approaches the strengthening area near the surface layer, where the strengthening points overlap more times, the friction coefficient is lower, and the wear type does not

change when the initial pressure is 75N. Therefore, the general trend of the friction coefficient of the sample black paint absorption lsp once by 75N shows that it fluctuates and decreases, and finally tends to be stable.

Figure 10-(b) shows friction coefficient of the friction process. In the friction process, the overall trend is the same as that of hardness, except for the early fluctuation. When the initial pressure is 75 N, after the friction coefficient is stable, there is a big fluctuation of black paint absorption LSP once, because of the lower surface hardness. And its main strengthening layer is near the surface layer, the friction coefficient is low in the area where the number of strengthening spot overlaps is more. After the initial fluctuation, the friction coefficient is stable at 0.4215. Because the friction area enters into the bottom layer of the spot area, the material hardness in this area is uniform, and the friction coefficient tends to be stable.

However, when the initial pressure is 100 N, this phenomenon does not appear. This is because the initial pressure increases, the friction process enters the near surface area with uniform hardness quickly. Therefore, when the initial pressure is 100 N, the friction coefficient curves fluctuate little. From the Fig. 10-(b), it can be seen that when the initial pressure is 75 N, compared with the initial pressure of 100 N, the friction coefficient is lower, and the trend is the same as the average friction coefficient.

4.2.4 Wear morphology

(1) Macro morphology by white light interference

Wear morphology was observed by white light interferometer, and wear volume was calculated. Fig. 11 shows the wear morphology and wear volume of under the 75 N and 100 N. Fig. 11-(a) shows wear morphology of raw materials. The wear surface is rough and has large lumps. The reason for this phenomenon is that the hardness of the material is relatively low, the flake will fall off under high load friction. In Fig. 11-(b) and (c), the depth of wear mark after LSP once is lower than that of three-times with black paint absorption layer. Moreover, there are more furrows in the wear morphology after LSP once. When the impact times are the same, the depth of wear mark with black paint absorption is lower than that no absorption. In Fig. 11-(i), the regularity of wear volume is the same as that of friction coefficient. This shows that the hardness increases, but the friction coefficient and wear volume decrease. When the initial load is 100 N, the regularity of wear morphology is the same as that of 75 N. As shown in Fig. 11-(i), the wear volume increases with the increase of initial pressure.

(2) Micro morphology by SEM

The wear morphology was observed by SEM. There are some oxides and carbides in the wear marks. Due to the deep wear marks, the material oxidizes to form iron oxide. Carbide is mainly the material and the hard phase in the grinding ball falls off and is rolled into the wear mark by the grinding ball. In Fig. 12-(a), there are mainly flake shedding and micro cutting marks in the wear morphology. In Fig. 12-(b), in addition to flake shedding, there are furrows and squashed abrasives in the wear morphology. The detached abrasive grains form three-body wear with the worn parts, thus forming furrow. At the same time, the exfoliated abrasive particles are rolled into the worn surface by GCr15 to form squashed

abrasives. In Fig. 12-(b), the wear mark surface is mainly micro cutting, furrows and abrasives. There are only some carbides in the wear marks. And the wear mark surface of LSP three-times no absorption is mainly micro cutting and a small amount of shedding. As the initial pressure increases, the quality of wear morphology decreases. As shown in Fig. 12-(e), (f), (g), and (h), the wear morphology has appeared the massive flakes. Due to the increase of load, there are more adhesive wear in the friction type, resulting in a large number of surface shedding. This is also the reason why the friction coefficient increases with increasing load.

The wear morphology was observed by SEM. There are some oxides and carbides in the wear marks. Due to the deep wear marks and the increase of temperature in the friction process, oxidative wear occurs on the wear mark surface, and the material oxidizes to form iron oxide. Carbide is mainly the material and the hard phase in the grinding ball falls off and is rolled into the wear mark by the grinding ball. In Fig. 12-(a), there are mainly flake shedding and micro cutting marks in the wear morphology. In Fig. 12-(b), in addition to flake shedding, there are furrows and squashed abrasives in the wear morphology. Different from the raw materials, the wear marks of LSP samples are reduced due to the increase of hardness. The phenomenon of peeling oxide layer exists, and the peeling oxide layer is rolled to the wear surface by GCr15, forming crushing abrasive. The oxide layer, which is not completely exfoliated, is separated in the process of friction, resulting in three-body wear between abrasive particles and worn parts, thus forming grooves. In Fig. 12-(b), the wear mark surface is mainly micro cutting, furrows and abrasives. And the wear mark surface of LSP three-times no absorption is mainly micro cutting and a small amount of shedding. Therefore, when the initial pressure is low, abrasive wear is dominant, and oxidation wear is accompanied in the wear marks. As the initial pressure increases, the quality of wear morphology decreases. As shown in Fig. 12-(e), (f), (g), and (h), the wear morphology has appeared the massive flakes. Due to the increase of load, there are more adhesive wear in the friction type, resulting in a large number of surface shedding. This is also the reason why the friction coefficient increases with increasing load.

4.3 Analysis and discussion

Through simulation and experiment, it is found that the hardness and residual stress of the H13 steel after three-times of LSP are higher than that the once LSP. This is due to the plastic deformation caused by high pressure shock wave and the increase of dislocation density caused by shock wave, resulting in grain refinement. Meantime, the effect of black paint absorption is better, especially the residual stress. In the aspect of friction coefficient, for the H13 steel with good strengthening effect, the friction coefficient is relatively low. And the early running in wear stage is relatively short. The friction coefficient is related to the surface quality and material properties of the friction pair, but not to the applied load. However, the friction coefficient is increased by 100 N. Through SEM, when the initial pressure is 100 N, there are more flakes appeared on the surface. The reason for this phenomenon is that as the load increases, the heat generated during the friction process also increases. And the wear type changes from simple abrasive wear to composite wear. The composite wear mainly includes abrasive wear and adhesive wear. The

change of wear type, especially the appearance of adhesive wear, directly leads to the deterioration of the friction pair surface, thereby increasing the friction coefficient.

5 Conclusion

(1) The results of LSP simulation show that the residual stress and the stress layer increase with the increase of LSP times and LSP pressure. In order to select the best experimental parameters, the LSP strengthening simulation is combined with the properties of raw materials. The residual stress of H13 steel is -420 MPa. Combined with the simulation, the optimal range of LSP pressure is 6-7 GPa.

(2) The results show that the residual stress of H13 is decreased after LSP without absorption layer. LSP without absorption layer absorbs laser energy, resulting in annealing of H13 surface and reduction of residual compressive stress.

(3) The LSP treatment shows that with the LSP times increase, the residual stress and the hardness increase. When the energy is 7 J, the spot diameter is 2.4 mm, and the LSP is 3 times, the residual stress and the hardness is the largest. Through the friction and wear experiment, it is found that the hardness increases, the friction coefficient and the wear volume decrease. The increase in friction load will not directly lead to an increase in friction coefficient. However, as the load increases, the type of wear appears adhesive wear, so the friction coefficient increases.

Declarations

Conflict of interest

The authors declared that they have no conflicts of interest to this work. We declare that we do not have any commercial or associative interest that represents a conflict of interest in connection with the work submitted.

Funding

This work is supported by The National Natural Science Foundation of China (51575234, 51872122), The Postdoctoral Science Foundation of China (2017M620286), The Key Research and Development Program of Shandong Province, China (2018CXGC0809), Major basic research projects of Shandong Natural Science Foundation (ZR2020ZD06), Project of Shandong Province Higher Educational Youth Innovation Science and Technology Program (2019KJB021), and Taishan Scholars and Youth Innovation in Science & Technology Support Plan of Shandong Province University.

Availability of data and material Transparent

Code availability Not applicable

References

1. Telasang G, Majumdar JD, Padmanabham G, Manna I (2015) Wear and corrosion behavior of laser surface engineered AISI H13 hot working tool steel. Surf Coat Technol 261:69–78. https://doi.org/10.1016/j.surfcoat.2014.11.058
2. Ren DJ, Shen JS, Chai JC, Zhou A (2018) Analysis of disc cutter failure in shield tunneling using 3D circular cutting theory. Eng Fail Anal 90:23–35. https://doi.org/10.1016/j.engfailanal.2018.02.015
3. Jia ZX, Liu YW, Li JQ, Liu LJ, Li HL (2015) Crack growth behavior at thermal fatigue of H13 tool steel processed by laser surface melting. Int J Fatigue 78:61–71. https://doi.org/10.1016/j.ijfatigue.2015.04.005
4. Dadoo A, Boutorabi SMA (2020) Correlation between pulsed laser parameters and MC carbide morphology in H13 tool steel/TiC composite coating. Opt Laser Technol 127:106120. https://doi.org/10.1016/j.optlastec.2020.106120
5. Yang HP, Wu XC, Cao GH, Yang Z (2016) Enhanced boronizing kinetics and high temperature wear resistance of H13 steel with boriding treatment assisted by air blast shot peening. Surf Coat Technol 307:506–516. https://doi.org/10.1016/j.surfcoat.2016.09.029
6. Liu B, Wang B, Yang XD, Zhao XF, Qin M, Gu JF (2019) Thermal fatigue evaluation of AISI H13 steels surface modified by gas nitriding with pre- and post-shot peening. Appl Surf Sci 483:45–51. https://doi.org/10.1016/j.apsusc.2019.03.291
7. Hu YX, Yang RY, Wang DY, Yao ZQ (2018) Geometry distortion and residual stress of alternate double-sided laser peening of thin section component. J Mater Process Technol 251:197–204. https://doi.org/10.1016/j.jmatprotec.2017.08.033
8. Wang H, Ning CY, Huang YH, Cao ZY, Chen XX, Zhang WW (2017) Improvement of abrasion resistance in artificial seawater and corrosion resistance in NaCl solution of 7075 aluminum alloy processed by laser shock peening. Opt Lasers Eng 90:179–185. https://doi.org/10.1016/j.optlaseng.2016.10.016
9. Ren NF, Yang HM, Yuan SQ, Wang Y, Tang SX, Zheng LM, Ren XD, Dai FZ (2014) High temperature mechanical properties and surface fatigue behavior improving of steel alloy via laser shock peening. Mater Des 53:452–456. https://doi.org/10.1016/j.matdes.2013.07.009
10. Angulo I, Cordovilla F, García-Beltrán A, Smyth NS, Langer K, Fitzpatrick ME, Ocaña JL (2019) The effect of material cyclic deformation properties on residual stress generation by laser shock processing. Int J Mech Sci 156:370–381. https://doi.org/10.1016/j.ijmecsci.2019.03.029
11. Cho KT, Song K, Oh SH, Lee YK, Lee WB (2013) Surface hardening of shot peened H13 steel by enhanced nitrogen diffusion. Surf Coat Technol 232:912–919. https://doi.org/10.1016/j.surfcoat.2013.06.123
12. Lu JZ, Lu HF, Xu X, Yao JH, Cai J, Luo KY (2020) High-performance integrated additive manufacturing with laser shock peening -induced microstructural evolution and improvement in mechanical properties of Ti6Al4V alloy components. Int J Mach Tool Manufact 148103475. https://doi.org/10.1016/j.ijmachtools.2019.103475

13. Prabhakaran S, Kalainathan S, Shukla P, Vasudevan VK (2019) Residual stress, phase, microstructure and mechanical property studies of ultrafine bainitic steel through laser shock peening. Opt Laser Technol 115:447–458. https://doi.org/10.1016/j.optlastec.2019.02.041
14. Shukla P, Nath S, Wang GJ, Shen XJ, Lawrence J (2017) Surface property modifications of silicon carbide ceramic following laser shock peening. J Eur Ceram Soc 37:3027–3038. https://doi.org/10.1016/j.jeurceramsoc.2017.03.005
15. Fabbro R, Fournier J, Ballard P, Devaux D, Virmont J (1990) Physical study of laser-produced plasma in confined geometry. J Appl Phys 68:775–784. https://doi.org/10.1063/1.346783

Figures

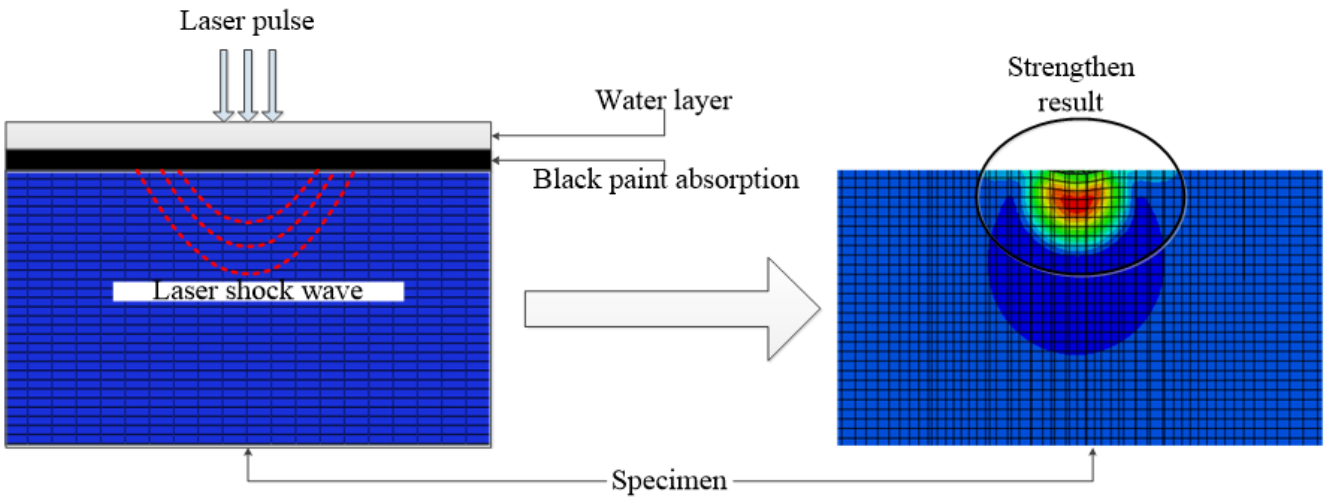

Figure 1

The schematic diagram of LSP theory

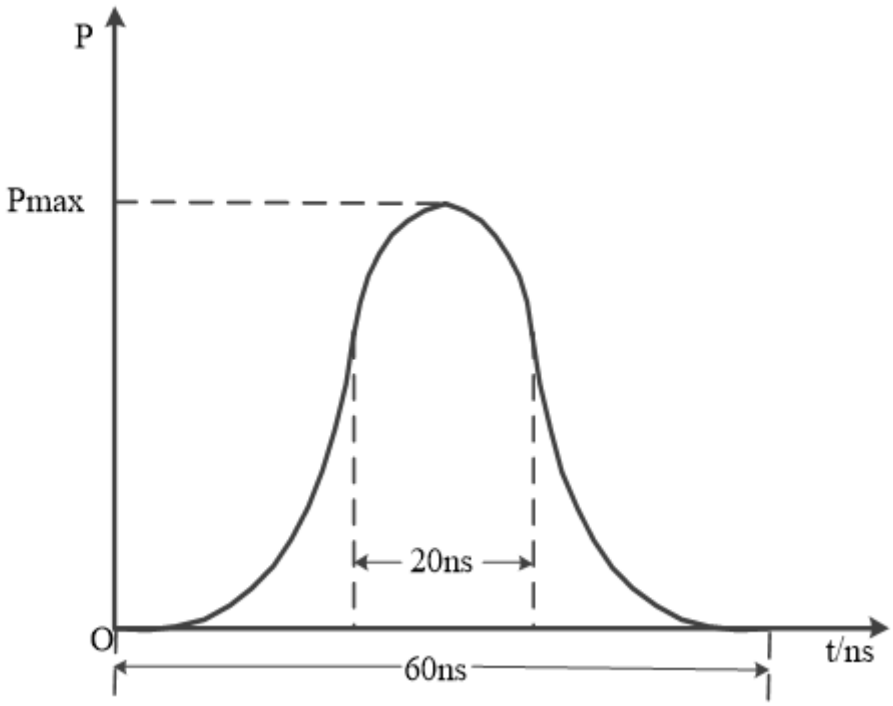

Figure 2

The pressure model of LSP

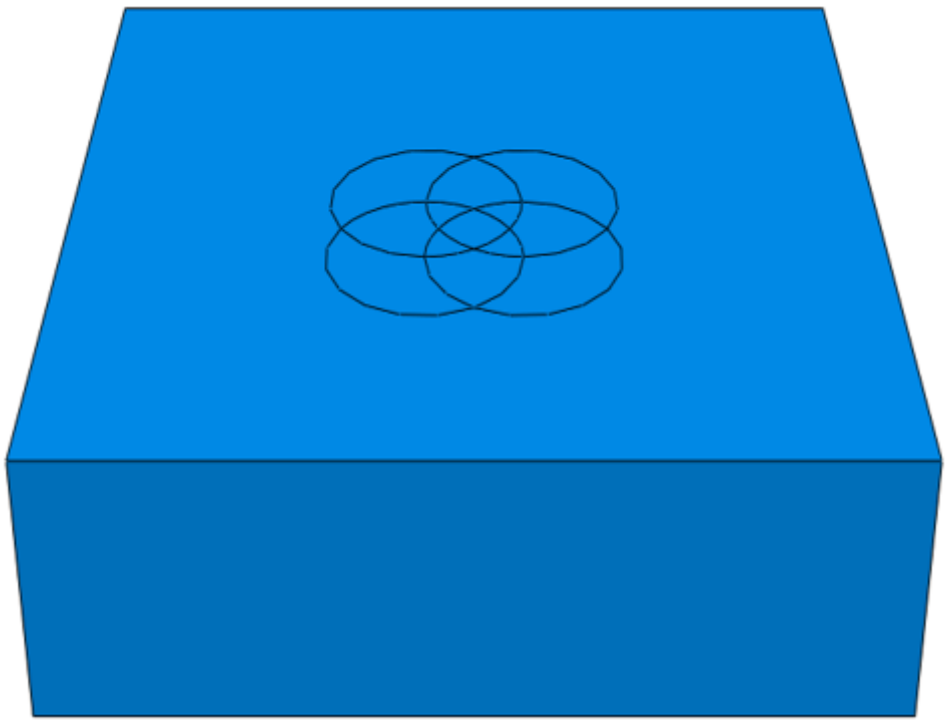

Figure 3

The simulation model of LSP

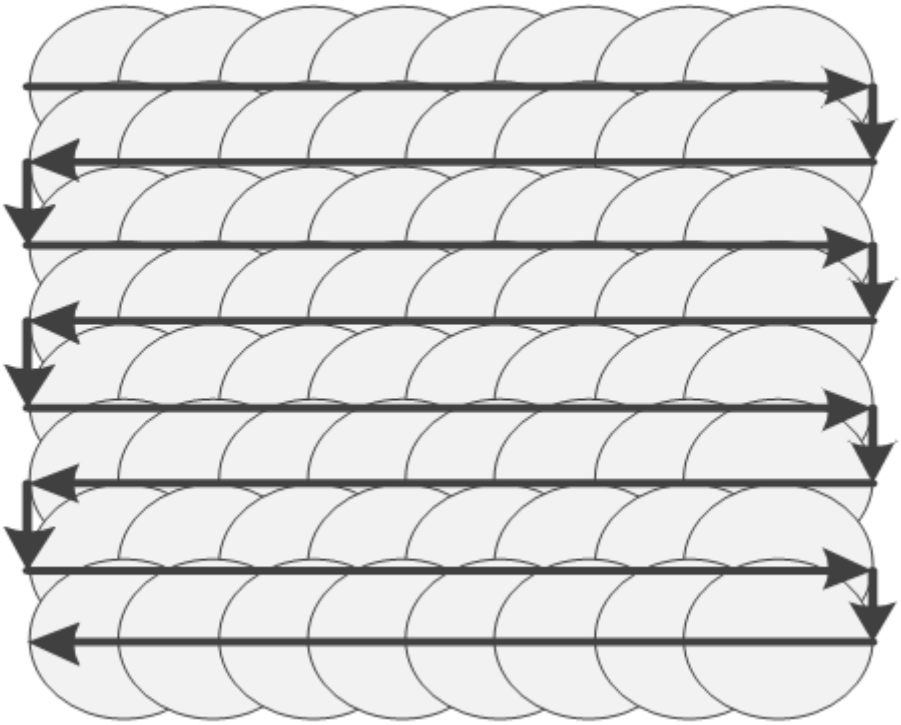

Figure 4

The processing path of LSP

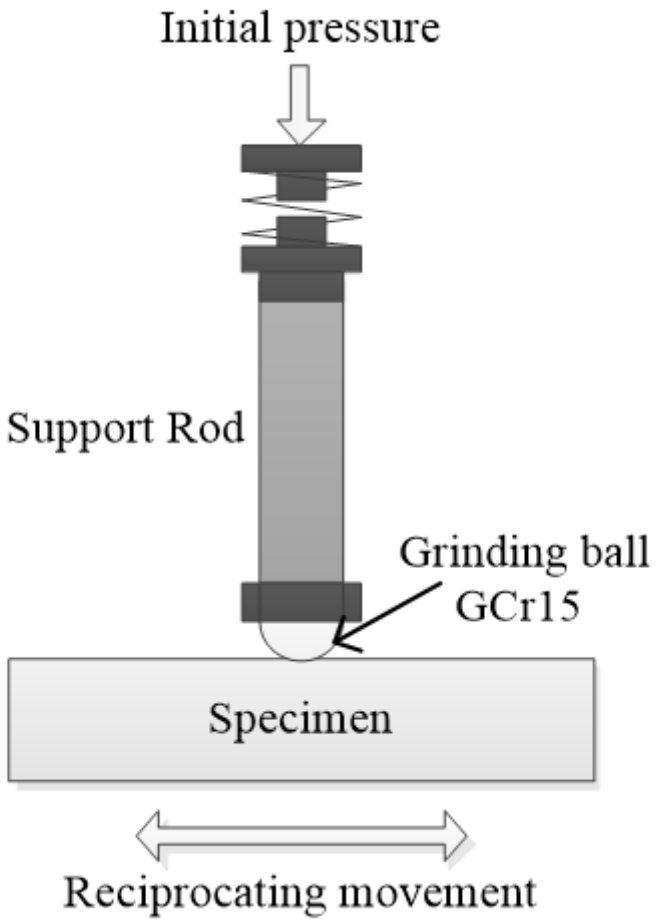

Figure 5

The schematic diagram of friction and wear tester

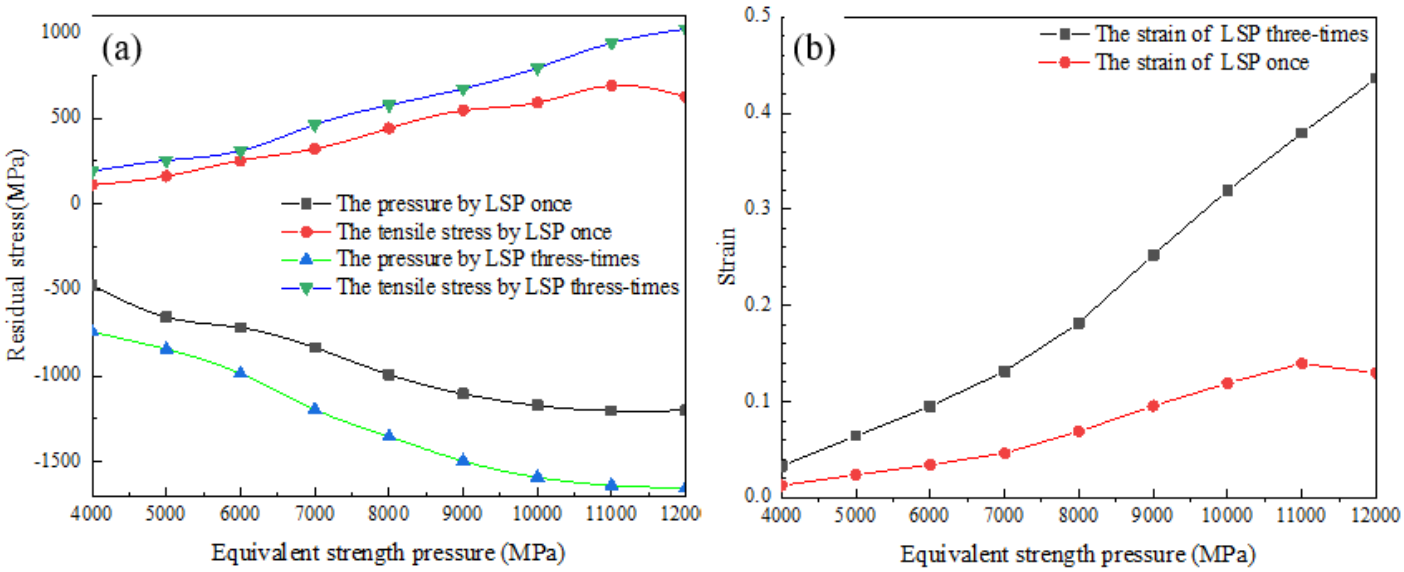

Figure 6

Residual stress and strain trend of LSP simulation: (a) Residual stress; (b) Strain.

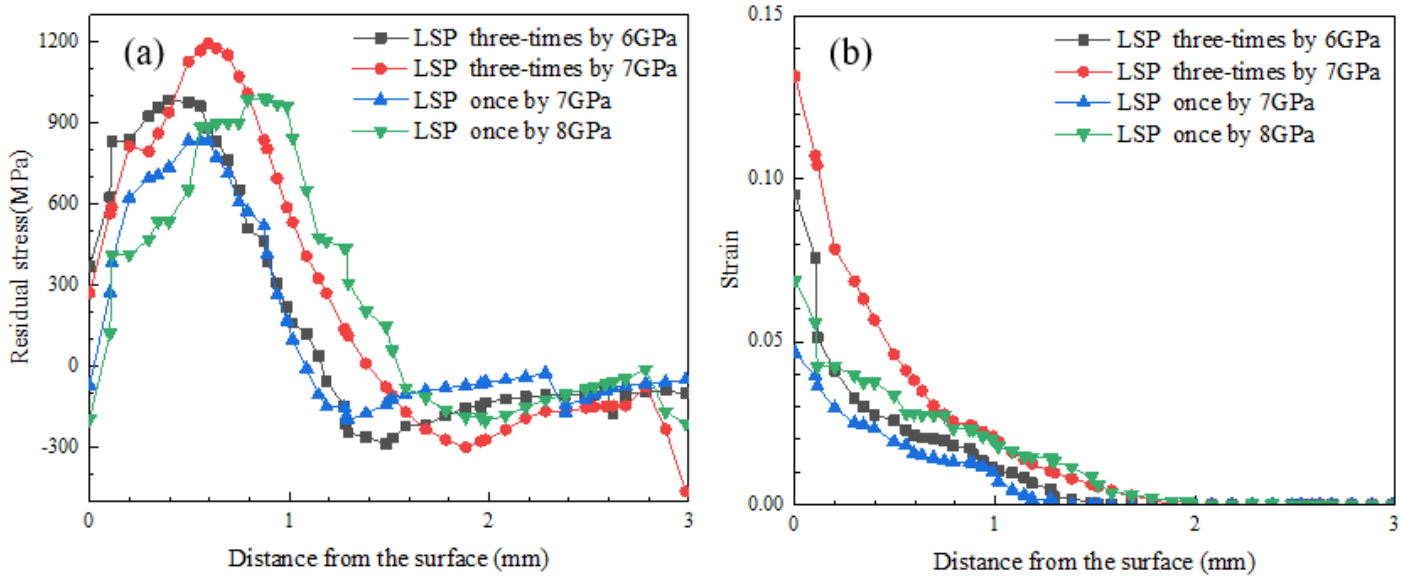

Figure 7

Residual stress and strain of different LSP pressure: (a) Residual stress; (b) Strain.

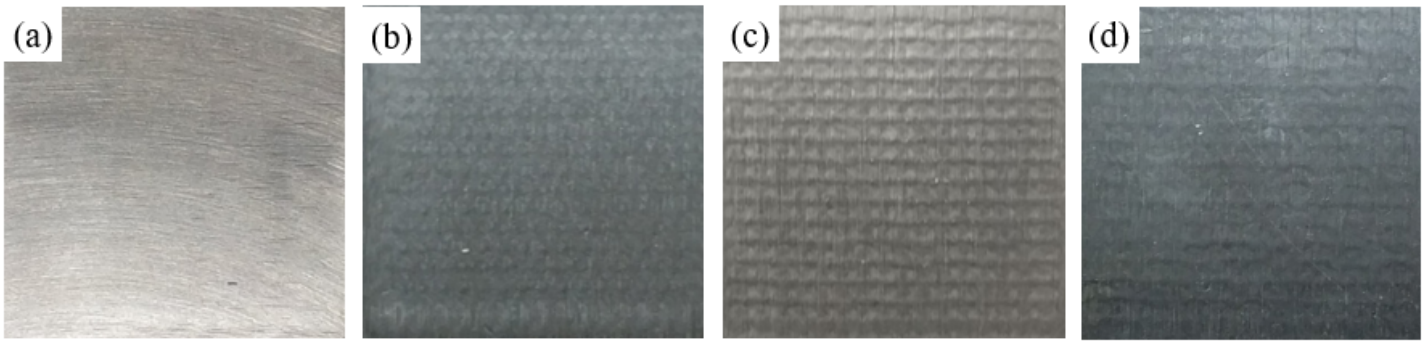

Figure 8

Surface morphology: (a) Surface morphology of raw material; (b) Surface morphology of black paint absorption LSP once; (c) Surface morphology of black paint absorption LSP three-times; (d) Surface morphology of no absorption LSP three-times.

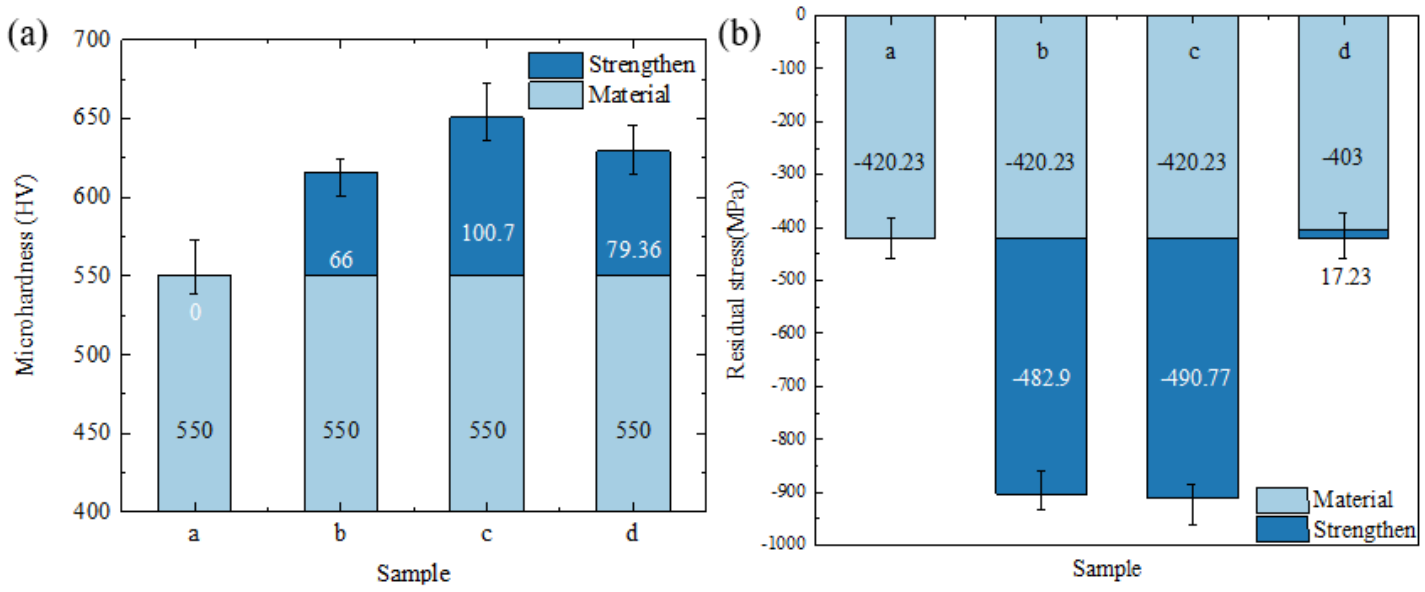

Figure 9

Micro-hardness and residual stress of LSP H13 steel: (a) Micro-hardness; (b) Residual stress.

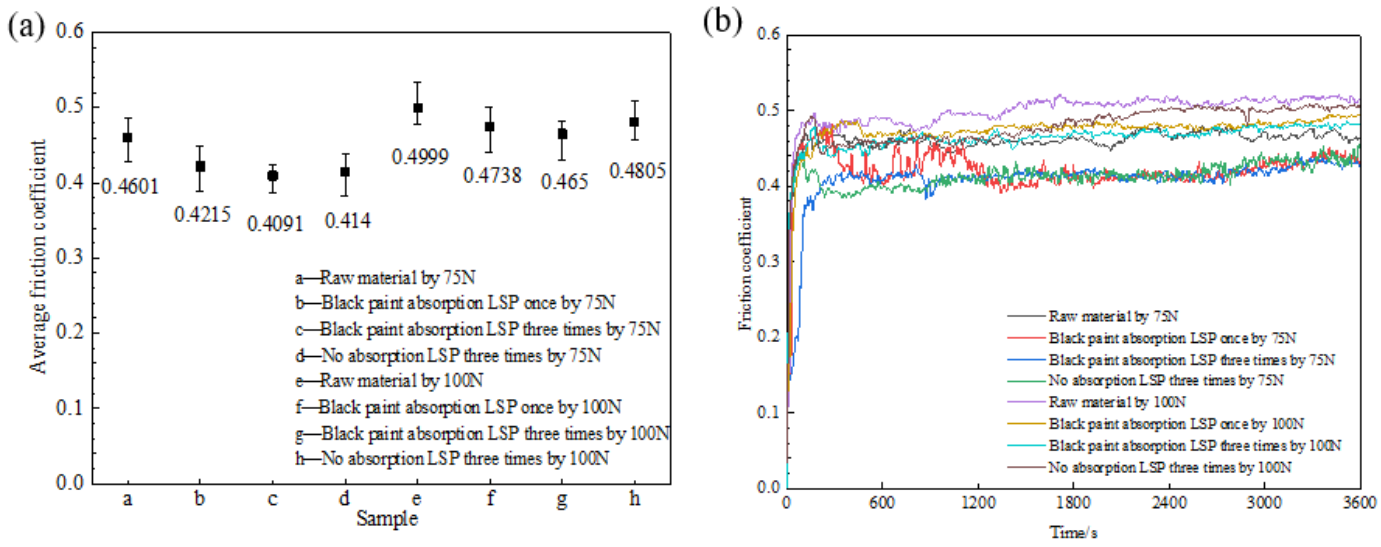

Figure 10

Average friction coefficient and friction coefficient of H13 steel: (a) Average friction coefficient; (b) Friction coefficient.

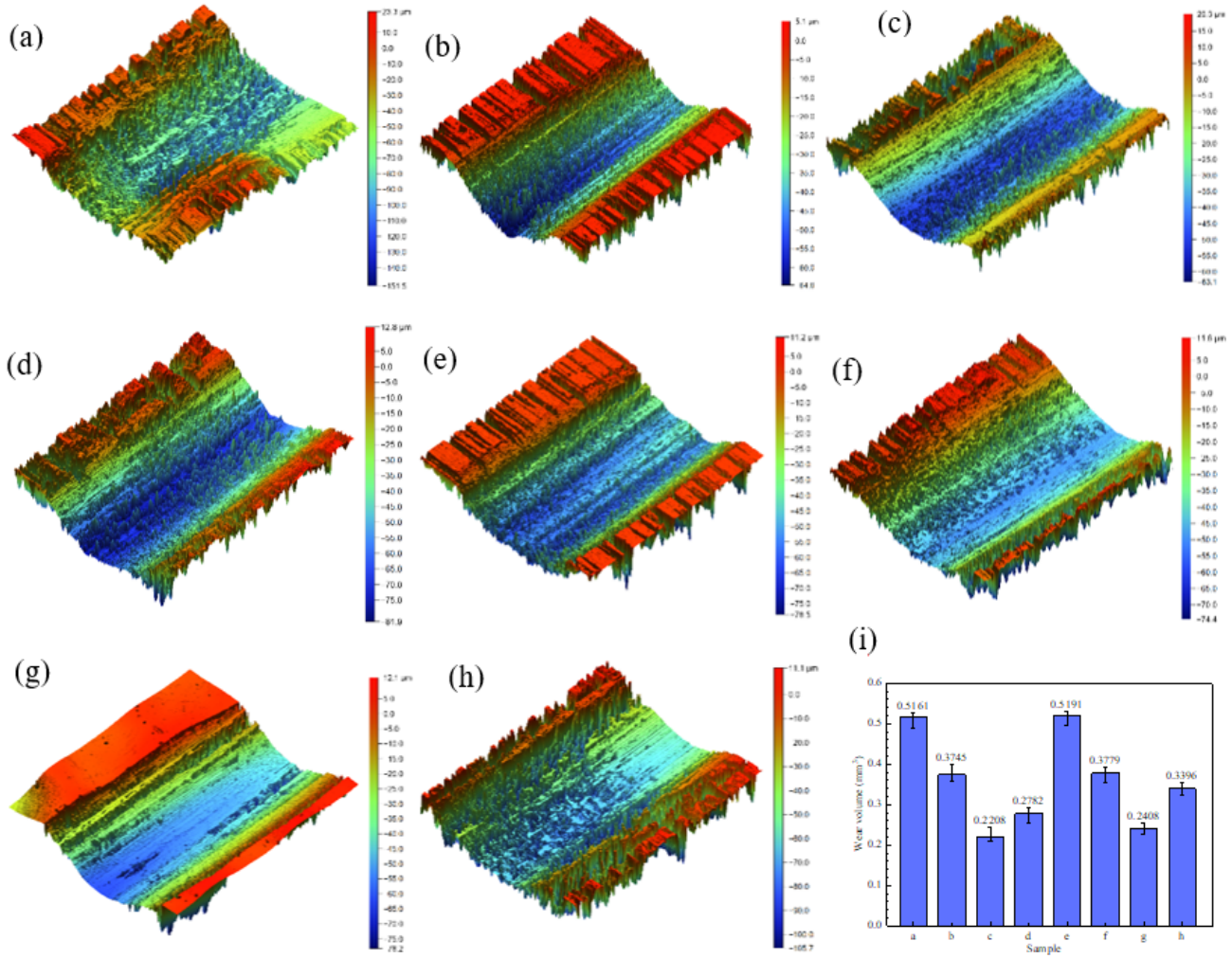

Figure 11

(a) Wear morphology of raw material by 75 N; (b) Wear morphology of black paint absorption LSP once by 75 N; (c) Wear morphology of black paint absorption LSP three-times by 75 N; (d) Wear morphology of no absorption LSP three-times by 75 N; (e) Wear morphology of raw material by 100 N; (f) Wear morphology of black paint absorption LSP once by 100 N; (g) Wear morphology of black paint absorption LSP three-times by 100 N; (h) Wear morphology of no absorption LSP three-times by 100 N; (i)Wear volume of (a)-(h).

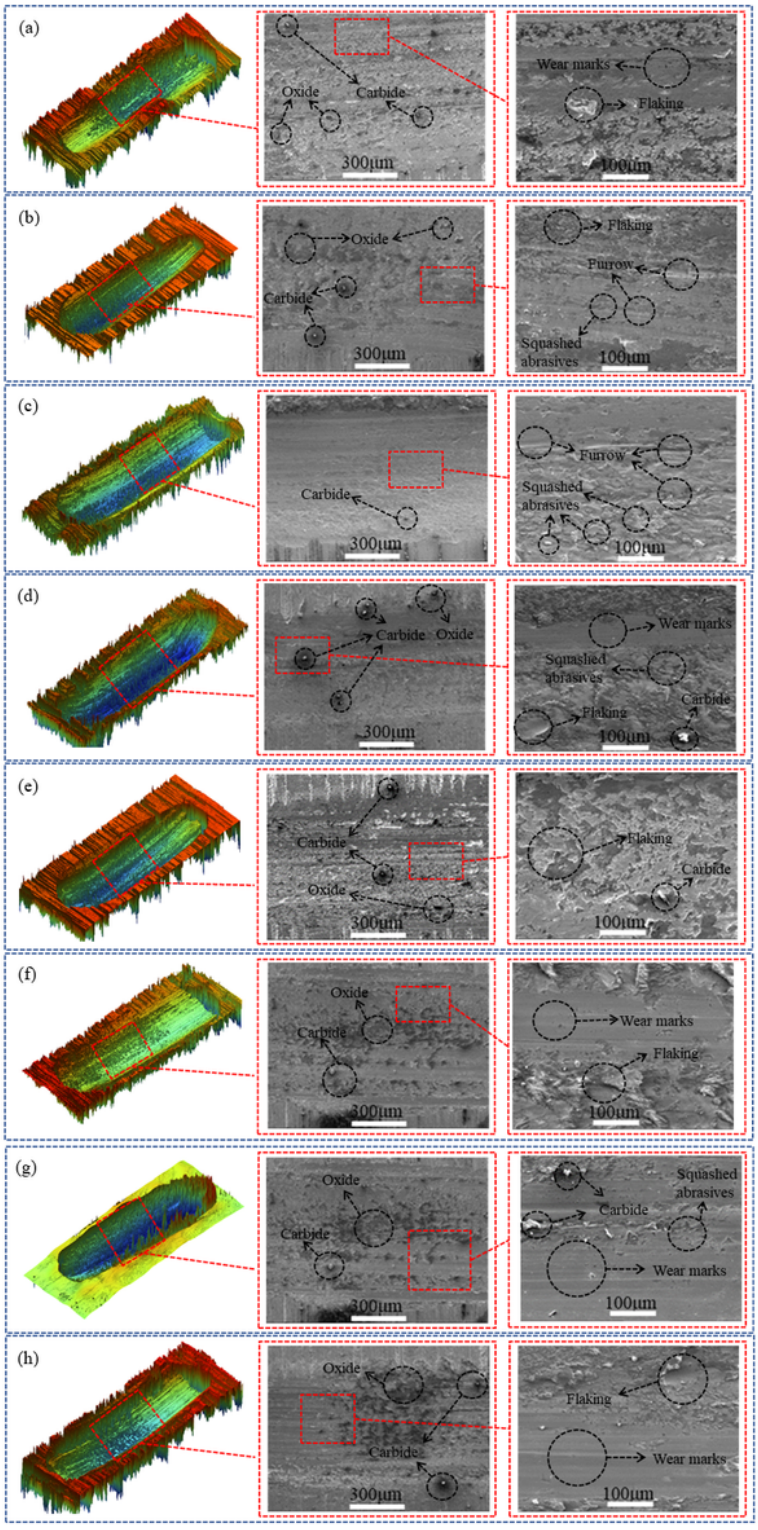

Figure 12

Wear micro morphology: (a) Wear morphology of raw material by 75 N; (b) Wear morphology of black paint absorption LSP once by 75 N; (c) Wear morphology of black paint absorption LSP three-times by 75 N; (d) Wear morphology of no absorption LSP three-times by 75 N; (e) Wear morphology of raw material by 100 N; (f) Wear morphology of black paint absorption LSP once by 100 N; (g) Wear morphology of

black paint absorption LSP three-times by 100 N; (h) Wear morphology of no absorption LSP three-times by 100 N.